Korean J. Chem. Eng., 40(2), 412-418 (2023)
DOI: 10.1007/s11814-022-1275-0

pISSN: 0256-1115
eISSN: 1975-7220

Vapor-phase synthesis of a robust polysulfide film for transparent, biocompatible, and long-term stable anti-biofilm coating

Hogi Kim*,‡, Seonghyeon Park*,‡, Younseong Song*, Wontae Jang*, Keonwoo Choi*, Kyoung G. Lee, Eunjung Lee*,†, and Sung Gap Im*,***,†**

*Department of Chemical and Biomolecular Engineering, KAIST, Daejeon 34141, Korea
**Nano-bio Application Team, National Nanofab Center (NNFC), Daejeon 34141, Korea
***KAIST Institute for the NanoCentury (KINC), Korea Advanced Institute of Science and Technology, Daejeon 34141, Korea
(*Received 27 July 2022 • Revised 23 August 2022 • Accepted 28 August 2022*)

Abstract−Biofilm formation caused by the fouling of microorganisms is one of the major problems in biomedical devices, food industry, and marine transportation. Since the removal of adherent biofilm is not a trivial task, it is of paramount importance to contain the formation of the anti-biofilm film. Herein, a polysulfide-based anti-biofilm coating (PAC) equipped with full transparency, non-toxicity, and environmental stability was developed via a simple vapor-phase synthesis. The polymer coating consists of polysulfide chain grafted onto poly (1,3,5,7-tetramethyl-1,3,5,7-tetravinyl cyclotetrasiloxane) (pV4D4) layer via thiol-ene click reaction, which was accomplished via a sequential deposition of each polymer followed by UV irradiation. The pV4D4 served as an adhesion promoter layer that substantially enhanced the interfacial adhesion between polysulfide layer and various substrate materials. The polysulfide layer exhibits a long-lasting anti-biofilm performance against pathogenic bacteria, such as *Escherichia coli: O157* and *Staphylococcus aureus*. The excellent anti-biofilm property is attributed to slippery surface derived from the non-adherent, dynamic characteristics of the polysulfide (-S-S-) chain. The anti-biofilm coating indeed shows outstanding durability and robustness when exposed to extreme pH, organic solvents, and mechanical stresses. The fully transparent, robust coating developed in this study is a promising candidate material for a broad range of anti-biofilm applications.

Keywords: Biofilm, Anti-biofilm Coating, Polysulfide, Slippery Surface, Initiated Chemical Vapor Deposition (iCVD)

INTRODUCTION

It is well recognized that microorganisms can attach to many arbitrary surfaces to form multicellular communities, called biofilms [1]. Most synthetic surfaces are quite vulnerable to microbial adhesion and biofilm formation, which often causes serious problems, such as surgical site infection [2], food poisoning [3], and increase of marine transport cost [4]. Since the biofilm is embedded in a resilient, chemical-resistant external matrix, called extracellular polymeric substances (EPS), removal of adherent biofilm is extremely challenging and labor-intensive [5]. Thus, instead of developing a removal method of biofilm, blocking the biofilm formation in early stage, or preventing the initial adhesion of microorganism becomes critically important [6]. Initially, the release of biocidal compounds was developed to eradicate the attachment of the microorganisms to the surface by killing or degrading them [7]. However, these strategies showed only short-period effect due to limited loading capacity, and have been restricted due to the potential environmental contamination by the release of toxic compounds [8].

A recent anti-biofilm strategy is to modulate the surface properties of the target substrates, such as topography, architecture, and surface chemical functionality, especially using polymer brushes [9], due to cost-effectiveness, non-toxicity, and their ability to form a thin coating to impart new surface properties [10]. Hydrophilic polymers such as polyethylene glycol (PEG) [11], polysaccharides [12], and zwitterionic polymers [13] are known to form a tightly bound hydration layer near the polymer brushes. Since the dehydration process by adhering fouling materials is thermodynamically unfavorable on the hydrated surface, hydrophilic polymer brushes are quite repulsive to the approach of foulants [14]. However, it has several limitations relating to long-term effectiveness and mechanical/chemical stability, which hamper the practical application of hydrophilic anti-biofilm coatings [15].

In case of hydrophobic polymer brushes, adsorption energy between foulants and surfaces is generally low; thus, foulants can be released easily by external stresses [16]. For the prevention of microbial adhesion, fouling-release strategies are widely accepted in which the foulant can be washed out through external stresses. Recently, robust superhydrophobic surfaces with complex surface structure have emerged as a potential solution for anti-biofilm surfaces [17]. However, realization of materials that persistently resist bacterial adhesion is not trivial to achieve by surface chemistry or surface structuring alone, because the nonspecific adsorption of proteins and surfactants secreted by bacteria often shields the underlying chemical functionality and thus loses anti-fouling performance [18]. Additionally, any defects in the surface chemistry could serve as nucleation sites for bacterial attachment. Especially, structured super-

†To whom correspondence should be addressed.
E-mail: ejung0608@kaist.ac.kr, sgim@kaist.ac.kr
‡Co-first authors.

hydrophobic surfaces in the Cassie (trapped air) state are prone to irreversible wetting (Wenzel transition), especially by the production of bacterial surfactants, which seriously limits their lifetime in underwater environments [19].

Unlike conventional surfaces, most of which are in rigid solid forms, synthetic hydrophobic anti-biofilm surfaces recently developed are often based on liquid or liquid-like dynamic surfaces [20] to create a surface that possesses dynamic features down to the nanometer scale, i.e., where the mobility of surface molecules or structures, may inhibit the permanent adherent status, thereby significantly disrupting the foulant adhesion. For example, Aizenberg and her colleagues developed a slippery surface inspired by the *Nepenthes* pitcher plant and have proven its excellent anti-biofilm properties [21]. The slippery surface exhibits superior anti-biofilm property with long-term stability under harsh conditions and self-healing property. However, the fabrication process of the dynamic surface is applicable only to specific types of substrate materials or requires complex substrate pretreatments. Moreover, they are prone to damage by mechanical or chemical stresses. Therefore, a facile fabrication method with novel materials to achieve robust anti-biofilm surface with long-term environmental stability is highly demanded.

The utilization of elemental sulfur might offer a new solution for the fabrication of novel anti-biofilm surfaces. Elemental sulfur is hydrophobic, chemically-resistant, and fifth most abundant element by mass on Earth [22]. Sulfur consists of several polyatomic bonds in which the bond cleavage/dissociation energy of S-S bond (430 kJ/mol) is only about two-thirds of that of the aliphatic C-C bond (607 kcal/mol), and thus the polysulfide (-S-S-) bonds are highly dynamic and susceptible to undergoing reversible chemical bond exchange at room temperature [23] (Fig. S1, Supporting Information). The rich variation of the dynamic covalent bond nature of the polysulfide chain makes sulfur-based materials self-healable [24] and lithium exchangeable for battery application [25]. In spite of such distinctive advantages of the sulfur-containing materials, the synthesis thereof is still quite challenging due to the extremely low immiscibility of sulfur with most organic compounds and the susceptibility of polysulfide chain to depolymerization to elemental sulfur [26]. Recently, we developed a new vapor-phase synthesis method of stable sulfur-containing polymer films [27]. Based on this synthesis technique, in this study we demonstrate that a hydrophobic polysulfide chain-based polymer film can effectively resist biofilm formation with high chemical stability. A dynamic but robust polysulfide chain was covalently grafted onto a vinyl-containing organosilicon polymer layer, which was deposited by using a solvent-free, low-temperature vapor-phase deposition process. The organosilicon layer served as an adhesion promotion layer to enhance the interfacial adhesion of the polysulfide film to target substrates. The vapor-phase process was capable of forming a conformal, transparent anti-biofilm coating on various target surface structures. The whole deposition process was performed at room temperature in a solvent-free way, which enabled the deposition of the anti-biofilm onto various arbitrary substrate materials without damaging them. The polysulfide-based coatings developed in this study exhibit outstanding anti-biofilm properties, transparency, biocompatibility, and excellent long-term durability against mechanical and chemical stresses.

MATERIALS AND METHODS

1. Fabrication of Polysulfide Anti-biofilm Coating (PAC)

Substrate materials, including glass, silicon wafer (Si), copper (Cu), poly(methyl methacrylate) (PMMA), poly(ethylene terephthalate) (PET), and polytetrafluoroethylene (PTFE), were sequentially cleaned in acetone, ethanol, and deionized water for 10 min prior to use. To provide vinyl functionality onto the surface, poly(1,3,5,7-tetramethyl-1,3,5,7-tetravinyl cyclotetrasiloxane) (pV4D4) film was synthesized *in situ* on the substrate from its corresponding monomer, V4D4 (Gelest, 95%) via the initiated chemical vapor deposition (iCVD) process. During iCVD process V4D4 was heated to 70 °C and introduced into the chamber (45 cm×45 cm (length and width)×10 cm (height)) at a flow rate of 0.91 standard cubic centimeters per minute (sccm) together with the initiator, *tert*-butyl peroxide (TBPO) (Aldrich, 97%). The flow rate of TBPO was kept at 0.5 sccm. The substrate temperature was maintained at 37 °C and the chamber pressure was set to 300 mTorr. The filament in the chamber was heated to 140 °C to cleave the initiator to radicals. The thickness of the deposited pV4D4 film was monitored *in situ* by a He-Ne laser (JDS Uniphase) interferometer.

After pV4D4 film deposition using iCVD, the substrates were exposed to sulfur vapor at atmospheric environment for the sulfur deposition. Then, sulfur-deposited substrates were treated by UV irradiation to induce a click reaction between vinyl groups within pV4D4 and the polysulfide chain. 254 nm of UV irradiation (VL-6-L.C, Vilber Lourmat) with a light intensity of 400 μW cm^{-2} was applied to the substrates directly and the distance from the substrate to UV light source was 88 mm. After the UV irradiation, the residual sulfur on the substrates was rinsed out via ultrasonication. All the chemicals in this study were used as received without further purification.

2. Characterization of PAC

Fourier transform infrared spectroscopy (FT-IR) spectra were obtained by ALPHA FTIR (Bruker Optics). The static/sliding contact angle was measured by a contact angle analyzer (Phoenix 150, SEO, Inc). The volume of an individual liquid droplet was 10 μL. The film thickness was measured using a spectroscopic ellipsometer (M2000, J. A. Woollam). The optical transmittance was measured using a UV-vis spectrometer (UV-3600m, Shimadzu) using a bare glass as a reference within the wavelength range of the visible spectrum. Atomic force microscope (AFM) images with a scan size of 5×5 μm were taken using a scanning probe microscope (PSIA XE-100, Park Systems). For the X-ray photoelectron spectroscopy (XPS) analysis (Thermo VG Scientific), a monochromatic Al K alpha source with a 220 mm beam diameter was used.

3. In vitro Anti-biofilm Assay

The bacteria species used in this study were *Escherichia coli* O157:H7 (*E. coli)* and *Staphylococcus aureus* (ATCC 29213) (*S. aureus)* donated kindly by Korea Research Institute of Bioscience and Biotechnology (KRIBB) (Daejeon, Korea). The strain was cultured on a constant temperature shaker (37 °C, 100 rpm) for 12 h after dilution in the sterilized Luria-Berani (LB) broth. The original bacterial solution was diluted with the LB broth to a concentration of 10^5 cell/mL, and then dropped onto the surface of samples including PAC, Polystyrene (PS) dish (SciLab Korea), Polyethylene

glycol (PEG; average molecular weight: 5000) grafted gold (Cytiva), and crosslinked polydimethylsiloxane (PDMS, Sylgard 184, Dow Hitech). To fabricate PDMS substrate, precursor of PDMS and crosslinker was mixed (10 : 1) and degassed, followed by annealing for 2 h at 90 °C. Each sample was cultured at 37 °C for 24 h to let the biofilm grow through the bacterial reproduction process. After the culture, the samples were slightly washed with phosphate buffered saline (PBS) for five times to remove the loosely attached bacteria. To observe the biofilm on the substrate, the biofilm was fixed with methanol and stained using bacteria viability kit (Thermo Fisher). The stained biofilm was then photographed using laser scanning confocal microscopy. To quantify the amount of the biofilm on the substrate, the fouling area was calculated based on the average areas of bacteria in microscopic pictures (n=10).

4. Cell Viability Assay

Normal human dermal fibroblasts (NHDFs) (Lonza) were cultured using Dulbecco's modified eagle medium (DMEM) containing 10% FBS (Welgene), 1% penicillin-streptomycin (Gibco). Cells were seeded on PAC and tissue culture polystyrene (TCPS) as control substrate at a density of 2×10^4 cells/cm^2. After culture for 24 h, cells were stained with calcein AM and ethidium homodimer-1 (Live/dead viability/cytotoxicity kit, invitrogen) following the manufacturer's instructions. Briefly, cells were washed with PBS and incubated with PBS containing about 2 μM calcein AM and 4 μM ethidium homodimer-1. After incubation for 30 minutes at room temperature, cells were imaged using fluorescence microscope (Nikon) (n=3). After viability test, cell viability was quantified as follows:

Cell viability=(Live cell proportion)/(Live+Dead cell proportion)×100 (%)

5. Film Stability Tests

For the mechanical and chemical stability tests, 100 nm-thick of the PAC were deposited on the substrates. After the stability test, anti-biofilm efficiency of the surfaces was quantified as follows:

Anti-biofilm efficiency
=(Fouling area of *E. coli* (1-day contact) before stability test)/
(Fouling area of *E. coli* (1-day contact) after stability test)×100 (%)

To evaluate the stability in mechanical stresses, anti-biofilm efficiency of the PAC was measured after immersion of the coatings into water and exposed to ultrasonication, water-flushing, and water-shearing treatments. In ultrasonicating test, tested samples (coating on Si wafer) were placed on a glass dish and immersed in water, followed by ultrasonication treatment with 20 kHz frequency without temperature control. In a water-flushing test, water flow was flushed perpendicularly to the tested samples (coating on Si wafer) and was cycled by a peristaltic pump with a flow rate of 10.0 mL/s. In water-shearing test, the samples (coating on Si wafer) were placed on the inner wall of the beaker and immersed in water, then subjected to the continuous shear rates (1,000 rpm) created by a stirring plate. To evaluate the chemical stability, the PAC were immersed into toluene, extreme pH buffer (pH 2 and pH 13), and hydrogen peroxide (H_2O_2, 30%) at room temperature for 1 day.

6. Statistical Analysis

All data were reported as the mean±SD. Statistical significance was assessed by unpaired student's *t*-test in case of 2 groups and two-way ANOVA for comparing three or more groups using GraphPad Prism Version 5.0 software (San Diego). A p-value<0.05 was considered statistically significant.

RESULTS AND DISCUSSION

1. Vapor-phase Synthesis of PAC

Fig. 1(a) shows a schematic diagram of the synthetic route of PAC through vapor-phase procedure. First, a monomer of 1,3,5,7-tetramethyl-1,3,5,7-tetravinyl cyclotetrasiloxane) (V4D4) with the initiator, *tert*-butyl peroxide (TBPO) was introduced in vapor phase

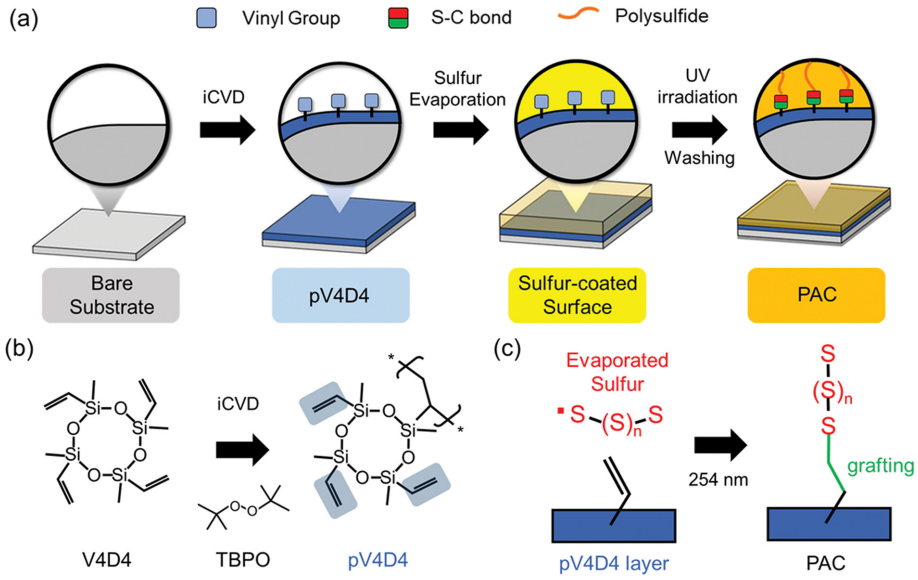

Fig. 1. Fabrication procedure of PAC. (a) Schematic overview for the fabrication process of PAC. (b) Chemical structures of V4D4 monomer, initiator (TBPO), and pV4D4 polymer. (c) Synthetic scheme of the photo-conjugation reaction between polysulfide chain and vinyl functionality.

to fabricate poly(1,3,5,7-tetramethyl-1,3,5,7-tetravinyl cyclotetrasiloxane) (pV4D4) layer using the initiated chemical vapor deposition (iCVD) process, where the polymer film grows directly from the surface of the substrates (Fig. 1(b)). An organosilicon layer with surface vinyl groups adheres strongly to arbitrary surfaces with high adhesion energy, promoting the interfacial adhesion of the polymer to target substrates [30]. Most importantly, the surface vinyl groups in the pV4D4 layer can function as the anchoring sites to graft polysulfide chains. On top of the adhesion promoter pV4D4 layer, polysulfide layer was deposited directly on the pV4D4-modified target substrate by thermal evaporation to grant anti-biofilm property to the substrate. Subsequently, the PAC-coated surface was exposed to UV irradiation to generate sulfur radicals from thermal homolytic ring opening of the evaporated sulfur, which in turn activates the surface vinyl functionality to form -S-C- bond, and completes the interfacial grafting of sulfur radicals to vinyl functionality on the pV4D4 layer (Fig. 1(c)).

Fig. 2(a) shows the representative optical images of the water contact angle (WCA) of bare glass, pV4D4-coated, sulfur-deposited, and PAC surfaces. When the substrate was coated with pV4D4 and sulfur, the hydrophilic glass substrate becomes hydrophobic. After the UV irradiation and rinsing the surface, a slight decrease of CA was observed, because the PAC surface became markedly smooth by the removal of the residual surface sulfur (Fig. S2, Supporting Information). The non-adherent property of the PAC surface was compared to the other substrates by measuring sliding angle (SA) using various liquids (Fig. 2(b)), including ethanol (EtOH), toluene, dimethyl sulfoxide (DMSO), deionized water, and human blood serum. All the liquid droplets now did slide off from the bare substrate, pV4D4 layer, and sulfur deposited layer with the tilting angle lower than 45°. On the other hand, PAC exhibits far smaller sliding angle (at least more than 30° difference) than pV4D4-coated surface, suggesting that the PAC showed better non-adherent property than other substrates. The PAC was applicable to arbitrary substrate materials including silicon wafer (Si), copper (Cu), poly(methyl methacrylate) (PMMA), poly(ethylene terephthalate) (PET), and polytetrafluoroethylene (PTFE) (Fig. S3, Supporting Information). The WCA measurements demonstrate that the non-adherent PAC surface exhibited a similar contact angle of 90° irrespective of the surface property of each substrate material, suggesting that the coating method is highly versatile and useful for the surface modification of various substrate materials (Fig. 2(c)).

2. Surface Characterization of the PAC

Vapor phase synthesis enabled the fabrication of ultrathin, transparent conformal thin film on target substrate. Fig. 2(d) shows the transmittance spectra of bare glass, pV4D4 films, sulfur, and PAC on a glass substrate. The 100-nm-thick PAC exhibits >99.0% transmittance over the entire visible light region, indicating its excellent optical transparency. In addition, the significant difference in transmittance between elemental sulfur film and PAC indicates that the excessive sulfur deposited on the pV4D4 was successfully removed through the ultrasonication-based washing process (Fig. S2, Supporting Information).

Fourier transform infrared spectroscopy (FT-IR) analysis of the

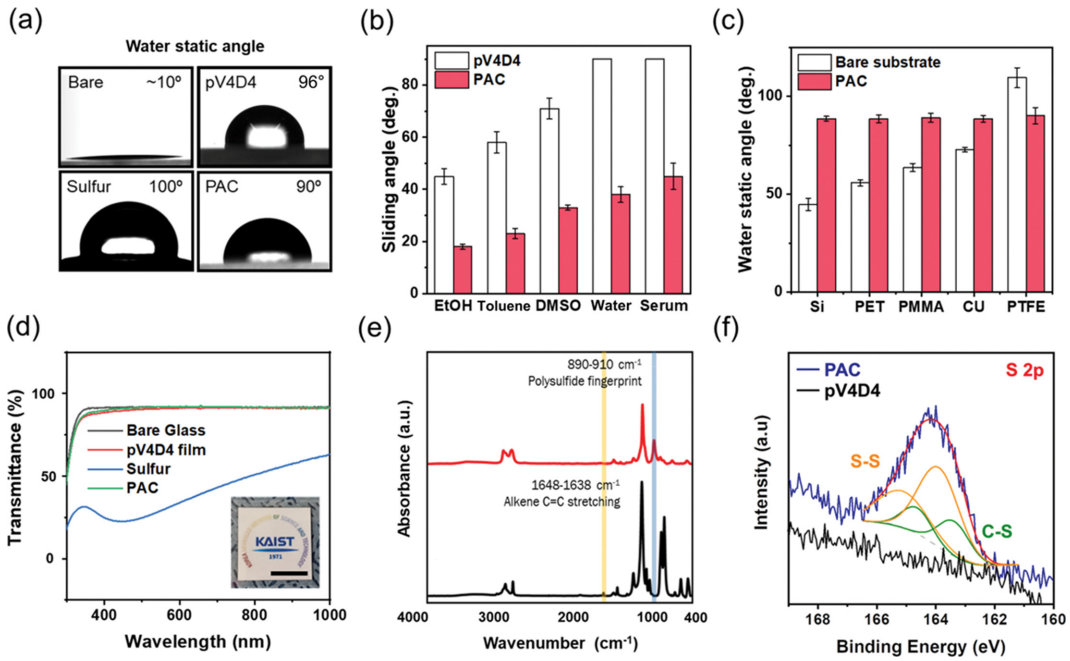

Fig. 2. Characterization of PAC. (a) Representative images of a 10 μL water droplet on bare glass, pV4D4-coated, sulfur-deposited, and PAC surfaces. (b) Measurement of sliding angle with 10 μL liquids with each surface energy on pV4D4 and PAC. (c) WCA of a 10 μL water droplet on the PAC coated on various substrates. (d) UV-Vis spectra of a bare glass, 100-nm-thick pV4D4 film coated on glass, 100-nm thick sulfur deposited on pV4D4 film, and PAC. Inset is optical photograph of the PAC on glass. Scale bar=1 cm. (e) Overall FT-IR spectra of pV4D4 and PAC. The yellow- and blue-shaded areas indicate the C=C stretching band around 1,640 cm^{-1} and the polysulfide fingerprint region at 900 cm^{-1}, respectively. (f) High-resolution XPS S2p scan spectrum of PAC (blue) and pV4D4 (black) on Si wafer and its deconvoluted peaks for S-S (orange) and bright green for C-S (green) bonds.

PAC was obtained to confirm the successful formation of grafted polysulfide chain (Fig. 2(e)). The peak around 1,640 cm^{-1} corresponding to the C=C stretching in the pV4D4 spectra disappeared, confirming the consumption of vinyl functionality by the UV-assisted reaction with polysulfide chain from the vapor-phase deposited sulfur film. The newly emerged broad band at roughly 900 cm^{-1} representing the polysulfide fingerprint region also confirmed successful grafting of polysulfide chain to the underlying pV4D4 films.

High resolution XPS analysis for sulfur element was also performed to investigate the surface chemical composition of PAC, where S2p peak was detected only from PAC surface, but not from the pV4D4 surface, which clearly indicates that the polysulfide brushes were formed on pV4D4 layer by the click conjugation reaction. The S2p peak was deconvoluted into two doublets, representing C-S and S-S bond at 164.6/163.4 eV and 165.1/163.9 eV, respectively (Fig, 2(f)) [29]. Estimated C-S to S-S ratio was 169 : 547, from which the average polysulfide chain length, or sulfur rank was determined to be 4.24. The analysis of PAC indicates the formation of dynamic polysulfide brushes grown from underlying organosilicon film, where the dynamic polysulfide brushes function as an anti-biofilm layer [31].

3. Biocompatible Anti-biofilm Properties of the PAC

The anti-biofilm property of the PAC surface was investigated by measuring the bio-fouling behavior of various microorganisms. To assess the non-adherent properties of the PAC surfaces to the biofilm formation, PAC and several other substrates including polystyrene (PS) with similar surface hydrophobicity with PAC, polydimethylsiloxane (PDMS), a conventional hydrophobic fouling-release material, and polyethylene glycol (PEG), a representative hydrophilic fouling-resistant material, were incubated with gram-negative bacteria, *Escherichia. Coli* O157:H7 (*E. coli*) and gram-positive bacteria, *Staphylococcus aureus* (*S. aureus*). Both of them are well-recognized as representative infectious pathogenic bacteria to cause biofilm formation, and subsequently resulting in the surgical site infection [32]. Figs. 3(a) and (b) show the scanning electron microscope (SEM) and fluorescence microscope images of each

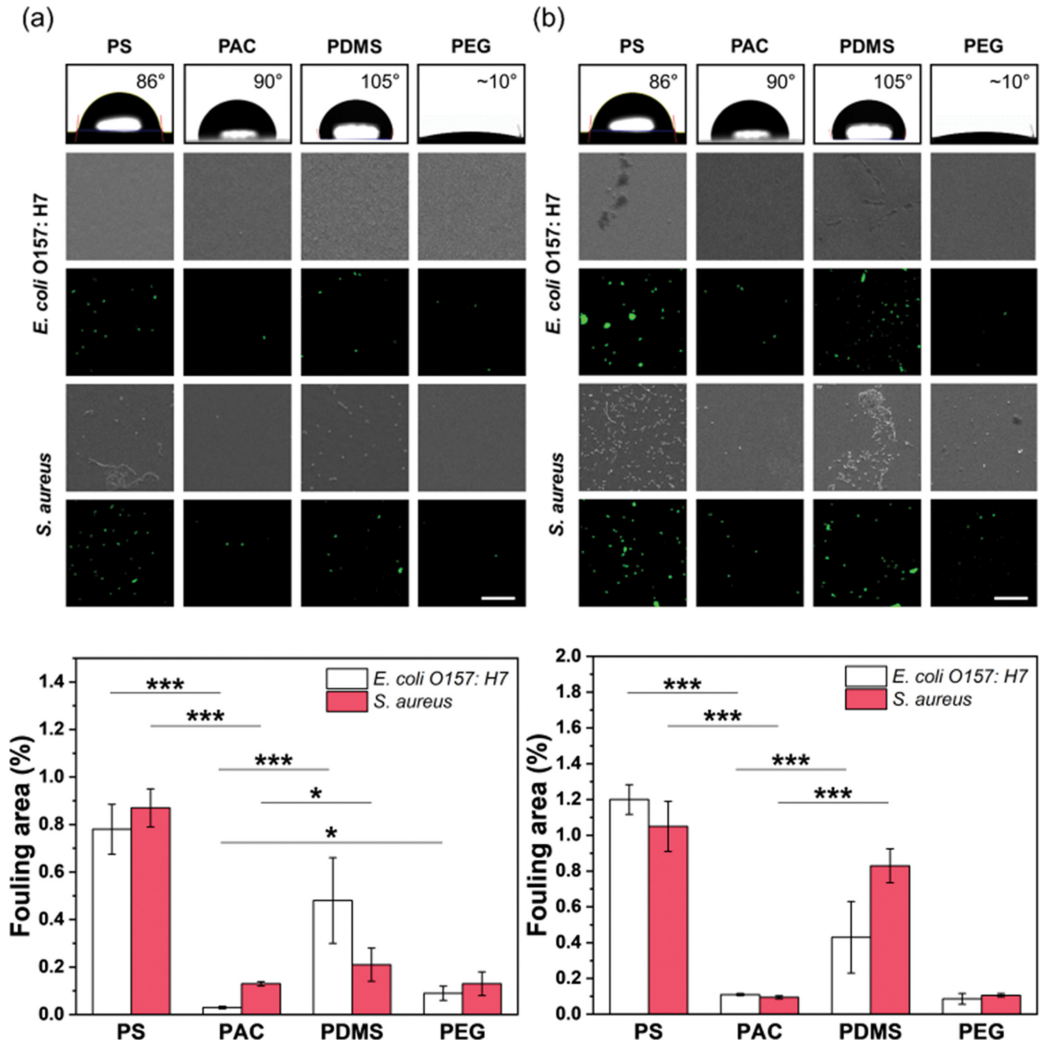

Fig. 3. Anti-biofilm performance of the PAC against pathogenic bacteria. Fluorescence microscope and SEM images of PS, PAC, PDMS, and PEG incubated in *E. coli* and *S. aureus* suspension for (a) 24 h and (b) 7 days at 37 °C. Scale bar=40 μm. Each graph below the images represents the anti-biofilm efficiency calculated by fluorescent intensity from each fluorescence microscope images (n=10 for each independent experiment; * p<0.05, ** p<0.01, *** p<0.005).

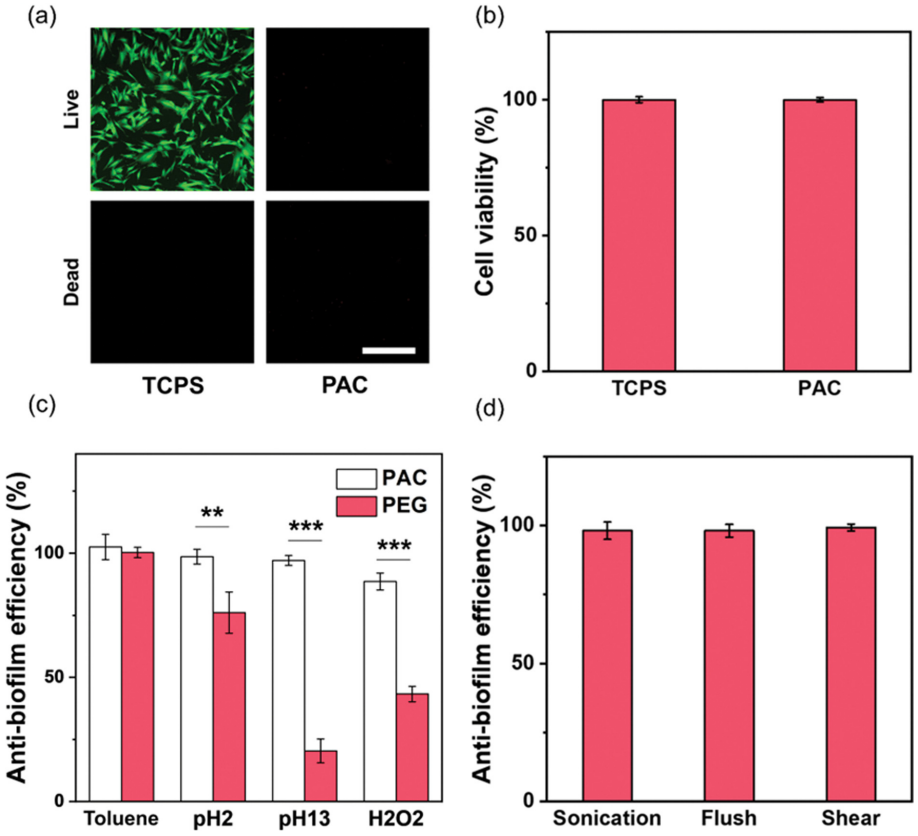

Fig. 4. (a) Live/dead assay of NHDFs cultured on TCPS and PAC. Scale bar=1 mm. (b) Cell viability of NHDFs cultured on TCPS and PAC. (c) Anti-biofilm efficiency of PAC after one-day exposure to various chemicals, including toluene, pH 2, and pH 13 solutions, and hydrogen peroxide (H_2O_2). (d) Anti-biofilm efficiency of PAC after i) one-day exposure to ultrasonication without temperature control; ii) seven-day exposure to perpendicular water flush; iii) 30-day exposure to water shearing (n=10 for each independent experiment; * $p<0.05$, ** $p<0.01$, *** $p<0.005$).

surface incubated in bacterial suspension for 24 h and 7 days. The *E. coli* adherent area on the PAC was 1.7 times, 10.3 times, 16.5 times lower than the PEG, PDMS, and PS, respectively, after 24 h incubation. Similarly, the *S. aureus* adherent area on the PAC was 1.9- and 7.3-times lower than the PDMS and PS, respectively, and comparable to that on PEG for 24 h incubation. After seven days incubation, PAC also maintained the outstanding anti-biofilm performance. The *E. coli* adherent area on the PAC was 4.3-times, 12.1-times lower than the PDMS and PS, respectively, and practically the same as that on PEG. The *S. aureus* adherent area on the PAC was 8.9-times, 10.3-times lower than the PDMS and PS, respectively, and similar to that on PEG. All these results clearly demonstrate that the PAC strongly inhibit the formation of the bacterial biofilm with long-term stability in aqueous environment. When examining the antifouling activities of two surfaces with similar hydrophobicity, PS and PAC, it was evident that the PAC surface showed far superior anti-biofilm performance. From these observations, we speculate that the anti-biofilm property of the PAC is attributed to the hydrophobic and dynamic nature of the polysulfide chain. The interfacial bond between hydrophobic surface and bacteria is weak due to low surface energy of PAC, so that the attached bacteria can be readily swept away by the hydrodynamic shear force. In addition, dynamic reconfiguration of S-S bond can easily release the adhered bacteria, thus imparting the anti-biofilm property to the PAC surface.

PAC-deposited tissue culture polystyrene (TCPS) was tested to examine the cytotoxicity of PAC itself against normal human dermal fibroblasts (NHDFs). Most of NHDF cells did not adhere to the PAC surfaces and easily washed out due to the strong anti-adherent properties of PAC (Fig. 4(a)). Some of NHDFs attached to the PAC surface were viable and no dead cells were observed, indicating the biocompatibility of hydrophobic PAC surface (Fig. 4(b)).

4. Chemical and Mechanical Stability of the PAC

For the practical application of anti-biofilm coating, it is crucial to secure the chemical and mechanical stability of the anti-biofilm coating on the substrate. The chemical stability of PAC was investigated by exposing the PAC to various chemicals including 1 M HCl, 1 M NaOH, and toluene at 37 °C for 24 h (Fig. 4(c)). Unlike the oxidation-susceptible PEG that exhibited over five-fold increase in the fouling efficiency, the PAC surface maintained more than 95% of its anti-biofilm property even after the exposure to the chemicals, demonstrating its outstanding chemical stability.

Mechanical durability of the PAC is also essential for practical anti-biofilm applications. The PAC was exposed to various mechanical stresses, including 1) water ultrasonication bath (20 kHz) without temperature control for 1 day, 2) continuous perpendicular water

flushing at a flow rate of 1.0 mL s^{-1} for 7 days, and 3) water shearing (1,500 rpm) at room temperature for 30 days (Fig. 4(d)). The surface characteristics of the PAC were well maintained even after they were exposed to those extreme environmental conditions (Fig. S4, Supporting Information). Additionally, the high mechanical durability of the PAC supports that the PAC preserve their original anti-biofilm property. These results verify that the PAC layer possesses a sufficient level of environmental robustness applicable to various biofilm-vulnerable devices.

CONCLUSIONS

A highly robust and biocompatible anti-biofilm coating was developed by incorporating dynamic polysulfide functionality onto a thin polymer coating via solventless vapor-phase deposition process. The vapor-phase synthesized polymer film exhibits both substrate-independent strong adhesion as well as excellent anti-biofilm capability against pathogenic bacteria and mammalian cells. The grafting of polysulfide chain could be achieved by UV-irradiation, which triggers the conjugation reaction between the sulfur chain and the surface vinyl functionality in pV4D4 layer with precise compositional control, imparting outstanding mechanical and chemical stability to the polysulfide layer. The newly developed polysulfide-based high-performance anti-biofilm surface, along with the scalability of the vapor-phase process, could pave the way for technologically mature anti-biofilm coatings with large-scale applicability.

ACKNOWLEDGEMENTS

Hogi Kim and Seonghyeon Park contributed equally to this work. This research was supported in part by National R&D Program through the National Research Foundation of Korea (NRF) funded by Ministry of Science and ICT (Grant No. NRF-2021M3H4A4079293), a grant from the Technology Innovation Program (No. 20008777) funded by the Ministry of Trade, Industry & Energy (MOTIE, Korea), and Nanomedical Devices Development Project of NNFC in 2022 (No. 1711160154). This study was also supported by the Basic Science Research Program through the National Research Foundation of Korea (NRF) funded by the Ministry of Education (No. 2020R1I1A1A01066621).

NOTES

The authors declare no competing financial interest.

SUPPORTING INFORMATION

Additional information as noted in the text. This information is available via the Internet at http://www.springer.com/chemistry/journal/11814.

REFERENCES

1. J. A. Shapiro, *Ann. Rev. Microbiol.*, **52**, 81 (1998).
2. A. G. Gristina, *Science*, **237**, 1588 (1987).
3. Y. Choi, Y. T. Kim, J. B. You, S. H. Jo, S. J. Lee, S. G. Im and K. G. Lee, *Food Chem.*, **270**, 445 (2019).
4. J. W. Costerton and P. S. Stewart, *Sci. Am.*, **285**, 74 (2001).
5. C. G. Kumar and S. K. Anand, *Int. J. Food Microbiol.*, **42**, 9 (1998).
6. K. K. Chung, J. F. Schumacher, E. M. Sampson, R. A. Burne, P. J. Antonelli and A. B. Brennana, *Biointerphases*, **2**, 89 (2007).
7. B. Meyer, *Int. Biodeterior. Biodegrad.*, **51**, 249 (2003).
8. L. Zhang, J. W. Yan, Z. W. Yin, C. Tang, Y. Guo, D. Li, B. Wei, Y. Xu, Q. R. Gu and L. M. Wang, *Int. J. Nanomedicine*, **9**, 3027 (2014).
9. C. M. Grozea and G. C. Walker, *Soft Matter*, **5**, 4088 (2009).
10. A. M. C. Maan, A. H. Hofman, W. M. de Vos and M. Kamperman, *Adv. Funct. Mater.*, **30**, 2000936 (2020).
11. S. Gon and M. M. Santore, *Langmuir*, **27**, 15083 (2011).
12. C. Yang, X. Ding, R. J. Ono, H. Lee, L. Y. Hsu, Y. W. Tong, J. Hedrick and Y. Y. Yang, *Adv. Mater.*, **26**, 7346 (2014).
13. W. F. Yu, Y. X. Wang, P. Gnutt, R. Wanka, L. M. K. Krause, J. A. Finlay, A. S. Clare and A. Rosenhahn, *ACS Appl. Bio Mater.*, **4**, 2385 (2021).
14. D. Y. Dong, C. Tsao, H. C. Hung, F. L. Yao, C. J. Tang, L. Q. Niu, J. R. Ma, J. MacArthur, A. Sinclair, K. Wu, P. Jain, M. R. Hansen, D. Ly, S. G. H. Tang, T. M. Luu and S. Y. Jiang, *Sci. Adv.*, **7**, eabc5442 (2021).
15. C. Leng, S. Sun, K. Zhang, S. Jiang and Z. Chen, *Acta Biomaterialia*, **40**, 6 (2016).
16. K. Chae, W. Y. Jang, K. Park, J. Lee, H. Kim, K. Lee, C. K. Lee, Y. Lee, S. H. Lee and J. Seo, *Sci. Adv.*, **6**, eabb0025 (2020).
17. Z. G. Guo, F. Zhou, J. C. Hao and W. M. Liu, *J. Am. Chem. Soc.*, **127**, 15670 (2005).
18. J. Genzer and K. Efimenko, *Biofouling*, **22**, 339 (2006).
19. R. Poetes, K. Holtzmann, K. Franze and U. Steiner, *Phys. Rev. Lett.*, **105**, 166104 (2010).
20. H. F. Bohn and W. Federle, *Proc. National Acad. Sci. United States Am.*, **101**, 14138 (2004).
21. A. K. Epstein, T. S. Wong, R. A. Belisle, E. M. Boggs and J. Aizenberg, *Proc. National Acad. Sci. United States Am.*, **109**, 13182 (2012).
22. T.-S. Wong, S. H. Kang, S. K. Y. Tang, E. J. Smythe, B. D. Hatton, A. Grinthal and J. Aizenberg, *Nature*, **477**, 443 (2011).
23. T. S. Kleine, R. S. Glass, D. L. Lichtenberger, M. E. Mackay, K. Char, R. A. Norwood and J. Pyun, *ACS Macro Lett.*, **9**, 245 (2020).
24. R. Martin, A. Rekondo, A. R. de Luzuriaga, P. Casuso, D. Dupin, G. Cabanero, H. J. Grande and I. Odriozola, *Smart Mater. Struct.*, **25**, 084017 (2016).
25. J. J. Griebel, N. A. Nguyen, S. Namnabat, L. E. Anderson, R. S. Glass, R. A. Norwood, M. E. Mackay, K. Char and J. Pyun, *ACS Macro Lett.*, **4**, 862 (2015).
26. R. Xu, I. Belharouak, J. C. M. Li, X. F. Zhang, I. Bloom and J. Bareno, *Adv. Energy Mater.*, **3**, 833 (2013).
27. J. J. Griebel, R. S. Glass, K. Char and J. Pyun, *Prog. Polym. Sci.*, **58**, 90 (2016).
28. D. H. Kim, W. Jang, K. Choi, J. S. Choi, J. Pyun, J. Lim, K. Char and S. G. Im, *Sci. Adv.*, **6**, eabb5320 (2020).
29. W. Jang, K. Choi, J. S. Choi, D. Kim, K. Char, J. Lim and S. G. Im, *ACS Appl. Mater. Interfaces*, **13**, 61629 (2021).
30. H. Kim, Y. Song, S. Park, Y. Kim, H. Mun, J. Kim, S. Kim, K. G. Lee and S. G. Im, *Adv. Funct. Mater.*, **32**, 2113253 (2022).
31. J. Liu, Y. L. Sun, X. T. Zhou, X. M. Li, M. Kappl, W. Steffen and H. J. Butt, *Adv. Mater.*, **33**, 2100237 (2021).
32. B. Y. Li and T. J. Webster, *J. Orthop. Res.*, **36**, 22 (2018).

Supporting Information

Vapor-phase synthesis of a robust polysulfide film for transparent, biocompatible, and long-term stable anti-biofilm coating

Hogi Kim[*,‡], Seonghyeon Park[*,‡], Younseong Song[*], Wontae Jang[*], Keonwoo Choi[*], Kyoung G. Lee[**], Eunjung Lee[*,†], and Sung Gap Im[*,*,†]**

*Department of Chemical and Biomolecular Engineering, KAIST, Daejeon 34141, Korea
**Nano-bio Application Team, National Nanofab Center (NNFC), Daejeon 34141, Korea
***KAIST Institute for the NanoCentury (KINC), Korea Advanced Institute of Science and Technology, Daejeon 34141, Korea
(*Received 27 July 2022 • Revised 23 August 2022 • Accepted 28 August 2022*)

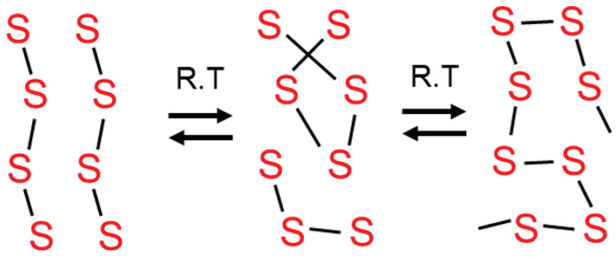

Fig. S1. Simplified representation of dynamic polysulfide exchange reaction at room temperature.

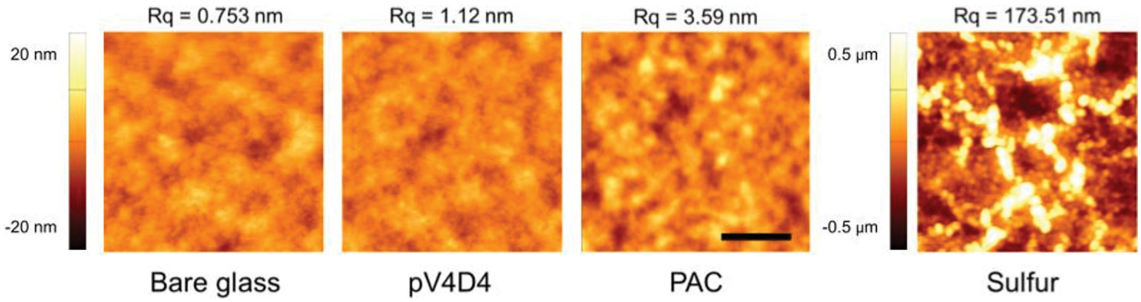

Fig. S2. AFM images of a bare glass, 100-nm pV4D4 coated glass, sulfur-deposited glass, and 100-nm PAC coated glass. Scale bar=1 μm.

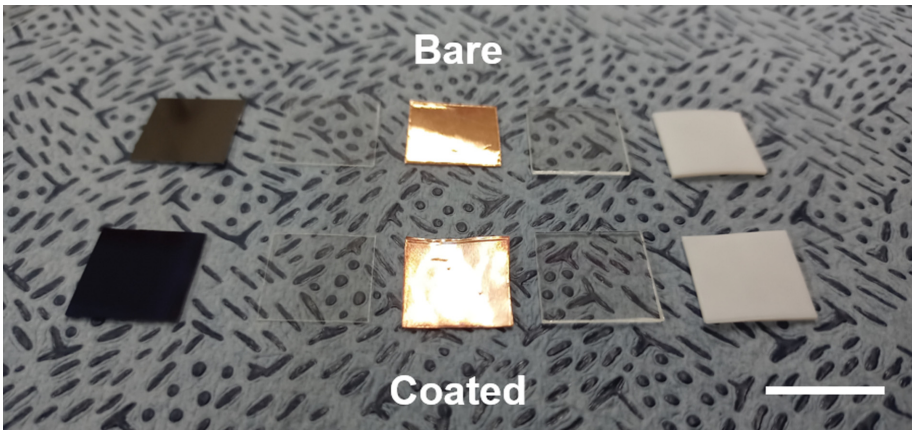

Fig. S3. Optical photograph of the PAC coated on on various substrate materials including glass, silicon wafer (Si), poly(ethylene terephthalate) (PET), copper (Cu), poly(methyl methacrylate) (PMMA), and polytetrafluoroethylene (PTFE) (from left to right) Scale bar=2 cm.

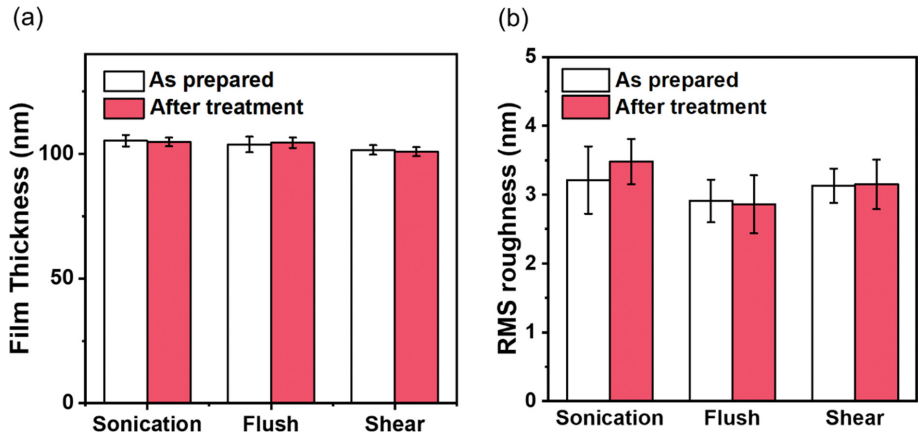

Fig. S4. (a) Thickness and (b) root mean square (RMS) roughness of PAC before and after mechanical stresses.